
ASYNCHRONOUS AVERAGING OF GAIT CYCLES FOR CLASSIFICATION OF GAIT AND DEVICE MODES

A PREPRINT

Parinaz Kasebzadeh

Department of Electrical Engineering
Linköping University
Linköping, Sweden
parinaz.kasebzadeh@liu.se

Gustaf Hendeby

Department of Electrical Engineering
Linköping University
Linköping, sweden
gustaf.hendeby@liu.se

Fredrik Gustafsson

Department of Electrical Engineering
Linköping University
Linköping, sweden
fredrik.gustafsson@liu.se

February 4, 2022

ABSTRACT

An approach for computing unique gait signature using measurements collected from body-worn inertial measurement units (IMUs) is proposed. The gait signature represents one full cycle of the human gait, and is suitable for off-line or on-line classification of the gait mode. The signature can also be used to jointly classify the gait mode and the device mode. The device mode identifies how the IMU-equipped device is being carried by the user. The method is based on precise segmentation and resampling of the measured IMU signal, as an initial step, further tuned by minimizing the variability of the obtained signature within each gait cycle. Finally, a Fourier series expansion of the gait signature is introduced which provides a low-dimensional feature vector well suited for classification purposes. The proposed method is evaluated on a large dataset involving several subjects, each one containing two different gait modes and four different device modes. The gait signatures enable a high classification rate for each step cycle.

Keywords Pedestrian dead reckoning, gait cycles, inertial measurement unit (IMU)

1 Introduction

Today, a variety of gadgets are attached to our bodies that contain an inertial measurement unit (IMU), for instance smartphones, smart watches, VR headsets, cameras, etc. There are also tailored solutions like foot-mounted IMUs for firefighters and IMU-equipped body suits used by e.g. the movie and gaming industry for virtual reality motion capture Chowdhury et al. [2018]. Besides solving dedicated tasks, these IMU signals also contain what will be referred to as the *gait signature* that is caused by the steps we take when moving. Examples include bio-mechanical analysis of limping patterns for diagnosis of certain diseases such as Parkinson's disease Caramia et al. [2018], and dead-reckoning for indoor positioning systems Ruiz et al. [2012], Tian et al. [2014], Davidson and Piche [2017], Jiménez et al. [2014]. We will refer to such classification tasks as determining the *gait mode*. The gait mode can also include bio-mechanical hypotheses of anomalies.

In most such studies, the position of the IMU on the body is known and decided by the application. Applications include foot-mounted IMUs for firefighters, head-mounted IMUs for VR glasses, wrist-mounted IMUs for smart watches, and IMUs for various fixed body parts in body suits Nilsson et al. [2014], Alvarez et al. [2012], Skog et al.

[2010], Zeng et al. [2018], Panahandeh et al. [2013]. For more general applications involving for example smartphones, the position might vary over time. We will refer to the position of the sensor on the body as the *device mode*.

There is a rich literature on the subject of using IMU signals for pedestrian dead reckoning (PDR) Basso et al. [2017], Jirawimut et al. [2003], Ho et al. [2016], Zihajehzadeh et al. [2015], Diez et al. [2018]. PDR is one application of gait analysis, which is typically solved by thresholding techniques, where e.g. the norm of the accelerometer is first band-pass filtered and then thresholded Brzostowski [2018], Norrdine et al. [2016], Kasebzadeh et al. [2016]. Using a fixed threshold typically leads to systematic errors for people heavier or lighter than the test subjects the threshold is designed for, and there are also false positive and negative step detections on the test subjects themselves. A third application of the gait signature is to improve step detection.

Step detection in PDR normally relies on zero velocity update (ZUPT) for lower-body mounted IMUs, such as foot-mounted applications. ZUPT is a typical, self-contained technique for step detection that benefits from the cyclical nature of human walking patterns and eliminates the bias from accelerometer and gyroscope Zeng et al. [2018], Skog et al. [2010], Norrdine et al. [2016]. However, extra care must be taken when dealing with upper-body sensors. The upper-body mounted or hand-held IMUs might report continuous or unexpected motion while the sensors in the lower body capture the foot at rest. Hence, instead of finding zero velocity periods as in ZUPT, step detection in PDR normally relies on peak detection or threshold-based approaches Renaudin et al. [2012], Kang and Han [2015].

Accurate step detection, hence, requires joint gait mode and device mode classification in order to get the proper threshold for the peak detection Pappas et al. [2001], Ho et al. [2016], Zhang et al. [2015, 2018]. An adaptive gait detection and step length estimation, based on walking speed classification, is proposed in Ho et al. [2016]. A probabilistic, user-independent method, as an alternative to threshold-based approaches, is introduced in Panahandeh et al. [2013] that uses chest-mounted IMUs to jointly perform gait analysis and classify the activity motions. A weighted context-based step length estimation algorithm using waist-mounted IMUs embedded in smartphones is proposed in Martinelli et al. [2018] which strives to classify six different pedestrian activities.

Existing approaches for step detection and gait cycle segmentation typically rely on measurements collected from hand-held devices such as smartphones that are already equipped with IMUs. Using such devices does not impose any extra cost and can become a universal solution Li et al. [2016], Kang and Han [2015]. However, due to the large number of factors affecting the sensor readings, such as the user's motion mode and the device mode, these methods suffer from robustness issues and might collapse if the underlying assumption is not satisfied. One solution to the problem is to classify the mode of the system and use the additional information obtained from this knowledge to robustify the algorithm.

The gait signature as observed by the IMU depends on both the gait mode (e.g. running, walking, strolling) and the device mode (for instance, a smartphone can be held in the hand, stored in a pocket or backpack, etc.), and as such reveals a rich information source suitable for a variety of applications. Our key contribution is a proposed algorithm for off-line analysis of IMU data during motion, with the following outline:

1. Gait segmentation using optimization to maximize similarity of the gait cycles. This step might need initialization, and here classical step detection algorithms can be used.
2. Estimation of the gait signature by averaging over the segments. This is done on a normalized time scale, so small variations in step cycle times are handled by resampling techniques.
3. Extraction of a low dimensional feature vector for the gait cycle using Fourier series analysis on the estimated gait signature. This feature vector includes physically explainable patterns.

This algorithm to estimate the gait signature is presented as an off-line one, although on-line versions are plausible. Thus, the gait signature estimation method can be used for either on-line classification, or off-line gait analysis.

The remainder of this paper is organized as follows: Sec. 2 describes the considered problem in detail. In Sec. 3, a standard threshold-based method for step detection is given followed by the solution to the gait cycle optimal segmentation problem. Sec. 4 presents a Fourier series approach to achieve a low-dimensional feature vector. The performance of the proposed method is evaluated in Sec. 5, which also includes an optional data pre-processing stage. Finally, the work is concluded in Sec. 6.

2 Problem Formulation and Notation

The most frequently used notations in this paper are summarized in Table 1.

Table 1: Notation

$\mathbf{x}(s)$	Noise-free data
$\mathbf{y}(s)$	Measured data
$\mathbf{e}(s)$	IMU measurement noise
$\hat{\mathbf{g}}_m(\tau)$	m :th gait cycle
$\bar{\mathbf{g}}(\tau)$	Gait signature
$\hat{\mathbf{G}}[l]$	Fourier series expansion of $\bar{\mathbf{g}}(\tau)$
N	Number of IMU samples
M	Number of gait cycles
L	Number of grid points of normalized time
s_n	Sample times of IMU
t_m	Step time for m :th gait cycle
τ	Normalized time $\tau \in [0, 1)$
ϵ_{lo}	Minimum gait cycle time
ϵ_{up}	Maximum gait cycle time
ϵ_p	Peak threshold
ϵ_v	Valley threshold

Consider some physical quantity $\mathbf{x}(s)$, possibly multi-dimensional, that depends on gait, which can be measured with additive noise $\mathbf{e}(s)$ as

$$\mathbf{y}(s_n) = \mathbf{x}(s_n) + \mathbf{e}(s_n), \quad n = 1, 2, \dots, N, \quad (1)$$

where s_n denotes the sampling times. We assume that the gait cycle is periodic over periods of time, and we are interested in the underlying average gait cycle of the physical quantity $\mathbf{g}(\tau)$ on a normalized time scale $0 \leq \tau < 1$. Fig. 1a is an example to represent periodic gait cycles over the normalized time scale. The presented data in Fig. 1a corresponds to a real scenario in which the walking subject was carrying a smartphone in the hand, facing upwards. All the gait segments in the figure were extracted manually from a bandpass-filtered accelerometer signal.

The challenge is to estimate the gait cycle $\hat{\mathbf{g}}(\tau)$ from the IMU measurements $\mathbf{y}(s)$, and the most critical step is the segmentation in which the signal is split into the separate gait cycles. We denote the beginning of each gait cycle time by t_m such that

$$s_1 \leq t_0 < t_1 < \dots < t_M \leq s_N. \quad (2)$$

Fig. 1b shows a histogram of step time duration, $t_m - t_{m-1}$, for all M gait cycles in Fig. 1a. Given these durations, we can obtain an estimate of the gait cycle, Fig. 1a, from each segment as

$$\hat{\mathbf{g}}_m(\tau) = \mathbf{x}(t_{m-1} + (t_m - t_{m-1})\tau), \quad \tau \in [0, 1). \quad (3)$$

Then, we immediately get what is referred to as an *asynchronously averaged* gait cycle by

$$\bar{\mathbf{g}}(\tau) = \frac{1}{M} \sum_{m=1}^M \hat{\mathbf{g}}_m(\tau). \quad (4)$$

The green line in Fig. 1a represents $\bar{\mathbf{g}}(\tau)$ for all manually extracted gait cycles.

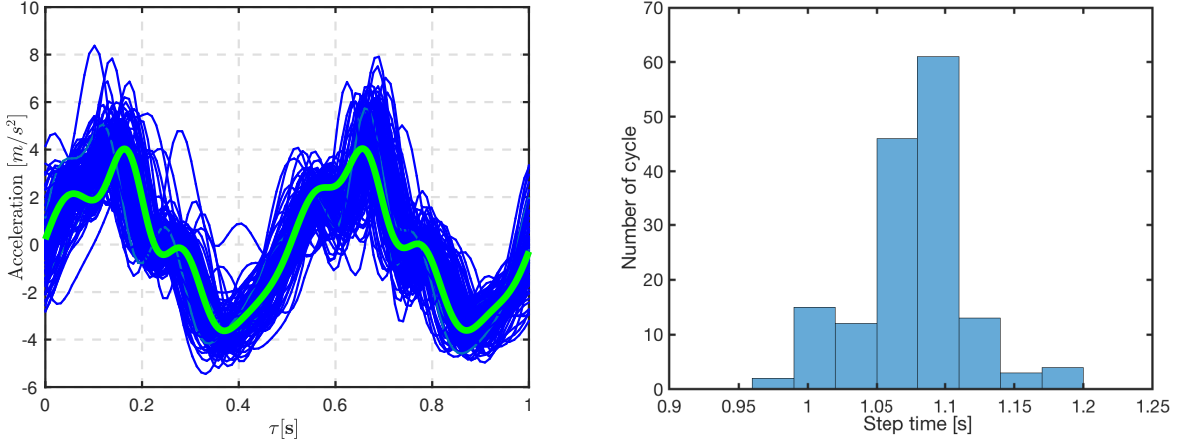
The key problem is thus to determine the step times such that different gait cycles $\hat{\mathbf{g}}_m(\tau)$ become as similar as possible. The considered metric as a measure of the similarity is the variance between each gait cycle and the averaged gait signature. We propose a nonlinear least squares framework where we optimize the step times in order to minimize the variance of these gait cycles

$$\hat{t}_{0:M} = \arg \min_{t_{0:M}} V(t_0:t_M), \quad (5a)$$

$$V(t_0:t_M) = \frac{1}{M} \sum_{m=1}^M \|\bar{\mathbf{g}}(\tau) - \hat{\mathbf{g}}_m(\tau)\|^2. \quad (5b)$$

To make the optimization problem mathematically tractable, we will approximate the optimization problem in the following ways:

1. The normalized time scale is discretized to L uniformly spaced grid points $\tau_l = (l-1)/L$ for $l = 1, 2, \dots, L$.



(a) Gait cycles, marked with blue lines, and averaged gait signature, marked with the green line.

(b) Histogram of step times.

Figure 1: Gait cycles, manually segmented using accelerometer signal.

2. The L_2 -norm is used in (5b), which gives a nonlinear least squares (NLS) problem, which often allows for efficient solvers.

Based on these assumptions, the problem can be written as

$$\hat{t}_{0:M} = \arg \min_{t_{0:M}} \frac{1}{LM} \sum_{m=0}^M \sum_{l=1}^L (\bar{g}(\tau_l) - \hat{g}_m(\tau_l))^2. \quad (6)$$

These two restrictions also enable us to formulate the signal Fourier series (FS) expansion in order to reduce the model order as introduced in Sec. 4.

A solution for this optimization problem is proposed in Sec. 3.1. Moreover, we will use a rather standard step detection method based on thresholding, outlined in Sec. 3.2, in order to initialize the optimization problem.

3 Optimal Segmentation of Gait Cycles

In this section, we first suggest a solution to the optimization problem (6). Then, a standard threshold-based step detection method is presented in order to initialize the optimization algorithm.

It is worth noting that all solutions are provided based on the assumption that the measurements are collected in advance (the solution is for the off-line mode). However, it could be easily extended to the on-line problems. Moreover, during the optimization process, all the gait cycles should be in the same regime of gait and device modes introduced in Table 2.

3.1 Solution for Optimization Problem

The sensor data should be band-pass filtered before segmentation to remove slow trends and high frequency noise. The cut-off limits in the band-pass filter should be selected to take the slowest and fastest pace into account –see Sec. 3.2 for further details. Moreover, the minimum step time ϵ_{lo} and the maximum step time ϵ_{up} are required to be defined in advance. These bounds can be obtained from the most frequent time interval of the gait cycles given by the histogram, *e.g.* Fig. 1b, of the detected gait cycles. The estimated step cycles should be in this interval.

The minimization problem for the objective function $V(t_0:t_M)$ is given by

$$\begin{aligned} & \underset{t_0:t_M}{\text{minimize}} && V(t_0:t_M) \\ & \text{subject to} && \epsilon_{lo} < t_m - t_{m-1} < \epsilon_{up} \end{aligned} \quad (7)$$

Algorithm 1 Proposed gait cycle segmentation algorithm**Input:** $\hat{g}(\tau)$, $\mathbf{t} = \{t_0:t_M\}$, ϵ_{lo} , ϵ_{up} and γ .**Output:** $\hat{\mathbf{t}} = \{\hat{t}_1:\hat{t}_M\}$.

```

1: Initialization:
   - Compute  $\bar{g}(\tau)$  using (4)
   - Compute  $V_1(t_0:t_M)$  using (6)
   - set  $i = 2$ 
2: repeat
3:   set  $m = 1$ .
4:   while  $m \leq M$  do
5:     Find  $\hat{t}_m$  using (10) for  $t_m$ 
6:     Replace  $t_m = \hat{t}_m$ 
7:     Update  $\bar{g}(\tau)$  using (4)
8:      $m = m + 1$ 
9:   end while
10:  Compute  $V_i(t_0:t_M)$  using (6)
11:  if  $V_i(t_0:t_M) - V_{i-1}(t_0:t_M) < \gamma$  then
12:     $\hat{\mathbf{t}} = \{\hat{t}_1:\hat{t}_M\}$ 
13:    Terminate the iterations.
14:  end if
15:   $i = i + 1$ 
16: until iterations are terminated.

```

In order to make the optimization procedure feasible, it is reformulated into M sub-optimal problems where each problem requires the optimal solution from the previous one. The first sub-problem is defined by

$$\begin{aligned} & \underset{t_1}{\text{minimize}} && V(t_0:t_M), \\ & \text{subject to} && \epsilon_{lo} < t_1 - t_0 < \epsilon_{up} \end{aligned} \quad (8)$$

where the outcome of the problem would be the optimal value of t_1 denoted by \hat{t}_1 . Given \hat{t}_1 , the second sub-problem becomes

$$\begin{aligned} & \underset{t_2}{\text{minimize}} && V(t_0, \hat{t}_1, t_2:t_M), \\ & \text{subject to} && \epsilon_{lo} < t_2 - \hat{t}_1 < \epsilon_{up} \end{aligned} \quad (9)$$

The optimized \hat{t}_2 is the outcome of the second step.

To generalize, the i :th $i \in [2, \dots, M]$ sub-problem is given by

$$\begin{aligned} & \underset{t_i}{\text{minimize}} && V(t_0, \hat{t}_1:\hat{t}_{i-1}, t_i:t_M). \\ & \text{subject to} && \epsilon_{lo} < t_i - \hat{t}_{i-1} < \epsilon_{up} \end{aligned} \quad (10)$$

These simplified optimization problems could be solved using a general linear search method algorithm which iteratively minimizes the cost function considering the given boundaries. Derivative-free quadratic interpolation and golden section search methods are used in this work Nocedal and Wright [2006].

Algorithm 1 outlines the proposed solution to find the optimal gait cycle segments from a given accelerometer signal. To initialize the algorithm, the preliminary gait cycles, $\hat{g}_{1:M}(\tau)$, are detected using a classical threshold-based step detection algorithm as described in Sec. 3.2. The initial signature, $\bar{g}(\tau)$, is then estimated by (4) considering all detected $\hat{g}_{1:M}(\tau)$. Subsequently, the cost function, $V(t_0:t_M)$, introduced in (5b) is computed using $\bar{g}(\tau)$ and $\hat{g}_{1:M}(\tau)$. For each gait cycle, $\hat{g}_i(\tau)$, the algorithm strives to find the optimal value \hat{t}_i using (10). Additionally, the initial gait signature is updated based on the new set of \mathbf{t} .

Once all the detected gait cycles have been optimized, the cost function, $V(t_0:t_M)$, will be re-computed given the estimated gait cycles. Henceforth, the new optimal gait cycles and updated signature will be used as the initialization for the next iteration of optimization problems. The termination criterion for this iterative algorithm is based on the decrement on the cost function. Hence, the algorithm will be iterate until the absolute decrease of cost function falls below the given threshold γ .

The performance of the optimization problem is evaluated for all introduced scenarios in Table 2 in Sec. 5.

3.2 Classical Gait Segmentation

To initialize the algorithm for offline applications, a threshold based step detection method is employed. A gait cycle, containing two consecutive toe-off moments of the same foot, can be crudely detected by defining two thresholds. If the peak threshold ϵ_p and the valley threshold ϵ_v are each crossed twice, then a cycle is taken. The measured signal will be compared against both ϵ_p and ϵ_v to find the time interval that it takes for the signal to cross both thresholds twice. Each gait cycle is then defined as sample values along this interval.

All the steps of the threshold-based step detection algorithm are summarized in Algorithm. 2. As a first step, in the gait cycle detection algorithm, we need to define the hyperparameter values for ϵ_p and ϵ_v . These values depend on human activity mode and device mode. Different approaches are introduced to consider proper thresholds, either pre-defined or adaptive Zhang et al. [2015], Kasebzadeh et al. [2016], Levi and Judd [1996]. In this work, pre-defined thresholds on norm of acceleration value have been used to detect peaks and valleys.

By considering a proper threshold for each scenario, the gait cycle can be extracted by comparing the norm of acceleration signal at each time with the ϵ_p or ϵ_v . Then, the upper bound or lower bound is hit as soon as $\|\mathbf{a}(k)\|$ becomes larger than ϵ_p or smaller than ϵ_v , respectively. Noting that each gait cycle contains two peaks and two valleys, c_{up} and c_{lo} are defined in order to count the number of times that the signal, $\|\mathbf{a}(k)\|$, hits the thresholds.

Peak and valley should be hit consequentially. However, we do not know which one comes first. Hence, in order to make sure that both peaks and both valleys have been detected in order, two flags hit_p or hit_v are defined. As soon as the first peak/valley has been hit, the corresponding flag hit_p or hit_v is set to TRUE and the other one will be FALSE. When both counters become larger than or equal to two, searching will stop and this part of the signal will be considered as a gait cycle. Finally, all counters are reset to initial values and the same procedure is repeated for the rest of the signal.

Algorithm 2 is applied to the experimental dataset (containing 8 scenarios), as introduced in Sec. 5 to get the gait cycle segmentations. The hyperparameter values are set to $\epsilon_p = 2 \text{ m/s}^2$ and $\epsilon_v = -2 \text{ m/s}^2$ for walking mode and $\epsilon_p = 4 \text{ m/s}^2$ and $\epsilon_v = -5 \text{ m/s}^2$ for running mode. The extracted segments are illustrated in Fig. 2. It is worth noting that all the gait cycle times are normalized such that $\tau \in [0, 1)$.

In this work, in order to extract the pattern of the gait cycle with better quality and to avoid bias drift, a pre-processing step is applied to the raw measured data. For this purpose, the signal is filtered through a fourth-order Butterworth filter with cut-off frequencies [0.1, 10] Hz to attenuate all frequencies outside the band-pass. The norm of the filtered signal is considered in this work in order to avoid unpredicted disturbances of the vertical acceleration that the orientation of the sensor may cause.

The initial gait signatures, $\bar{\mathbf{g}}(\tau)$, computed by (4) are plotted over the detected gait cycles for all the scenarios and indicated with thick green line in Fig. 2. As the figures suggest, although a general pattern is visible for the extracted gait cycles in all scenarios, further tuning is required. For example, when the device is in swinging mode, Fig. 2c and Fig. 2d, corresponding to walking and running with swinging hand, the gait cycles are very noisy and there are some misdetections of gait segments. Moreover, in ‘‘W4’’ scenario, presented in Fig. 2g, corresponding to walking with backpack device mode, there is some shifting. In the running activity mode the patterns are quite noisy and the lengths of the cycle times also vary as shown in the histograms corresponding to running gait modes.

Unexpected behaviors in the motion and the device modes are unpredictable and always exist in pedestrians’ daily activities. Hence, these classical algorithms such as the one given by Algorithm 2 should be complemented by more advanced methods.

The introduced optimal segmentation in Sec. 3.1, suggests a solution to take care of unexpected behaviors and reduce the rate of error. The performance of the proposed method is evaluated on a large dataset and presented in Sec. 5.

4 Data Reduction with Fourier Series

In this section, we are looking for a low order approximation, which can be recasted as a least squares (LS) estimation problem using a linear regression framework.

Given our sequence of step times and the measurement noise we have for each $\hat{g}_m(\tau_l)$, we strive to find a parametric model, using a linear regression framework, of the average $\bar{g}(\tau_l)$. We show that the parameters of the fitted model provide a useful set of features for future classification purposes.

Algorithm 2 Gait cycle detection**Input:** Norm of accelerometer signal

$$\|\mathbf{a}(k)\| = \sqrt{\mathbf{a}_x^2 + \mathbf{a}_y^2 + \mathbf{a}_z^2}.$$

- Lower bound ϵ_{lo} and upper bound ϵ_{up} thresholds, if hit step is occurred**Output:** Set of gait cycles $\{Y_m\}_{m=1}^M$

1: Initialization:

- Set counters $c_{up} = 0$ and $c_{lo} = 0$ representing the number of times upper and lower bounds are hit- set $hit_p = \text{FALSE}$ and $hit_v = \text{FALSE}$ - $k_{start} = 1$ - $k = k_{start}$ - $m = 1$ 2: **repeat**3: **if** $\|\mathbf{a}(k)\| \geq \epsilon_{up}$ **then**4: $c_{up} = c_{up} + 1$ 5: $hit_p = \text{TRUE}, hit_v = \text{FALSE}$ 6: **end if**7: **if** $\|\mathbf{a}(k)\| \leq \epsilon_{lo}$ **then**8: $c_{lo} = c_{lo} + 1$ 9: $hit_p = \text{FALSE}, hit_v = \text{TRUE}$ 10: **end if**11: $k = k + 1$ 12: **until** $hit_p = \text{TRUE}$ or $hit_v = \text{TRUE}$ 13: **while** $c_{up} < 2$ and $c_{lo} < 2$ and $k \leq N$ **do**14: **if** $\|\mathbf{a}(k)\| \geq \epsilon_{up}$ and $hit_p = \text{FALSE}$ and $hit_v = \text{TRUE}$ **then**15: $c_{up} = c_{up} + 1$ 16: $hit_p = \text{TRUE}, hit_v = \text{FALSE}$ 17: **end if**18: **if** $\|\mathbf{a}(k)\| \leq \epsilon_{lo}$ and $hit_p = \text{TRUE}$ and $hit_v = \text{FALSE}$ **then**19: $c_{lo} = c_{lo} + 1$ 20: $hit_p = \text{FALSE}, hit_v = \text{TRUE}$ 21: **end if**22: $k = k + 1$ 23: **end while**24: $\{Y_m\} = \|\mathbf{a}(k_{start} : k - 1)\|$ 25: $\{t_m\} = t_{acc}(k - 1)$ 26: $k_{start} = k$ 27: $m = m + 1$ 28: $c_{up} = 0$ and $c_{lo} = 0$ 29: **return** $\{Y\}, \{t\}$

In order to extract a low dimensional feature vector for the gait cycle using estimated signatures, we apply FS expansions to the gait segment from the sampled version of the gait cycle $\hat{G}_m[l], l = [0, 1, \dots, L - 1]$

$$\hat{G}[l] = \sum_{k=0}^{K-1} a_k \cos(2\pi\tau_l k) + b_k \sin(2\pi\tau_l k), \quad (11)$$

where the parameter set $\{a_k, b_k\}_{k=1}^K$ forms the feature space used to identify each particular gait mode and K is the model order. As in any other regression model, the trade-off between model complexity and accuracy cannot be neglected. In order to estimate the FS coefficients, for each model order K , the Fourier series expansion (11) is considered as a linear model given by

$$\bar{g} = \mathbf{H}_K \boldsymbol{\theta}_K, \quad (12)$$

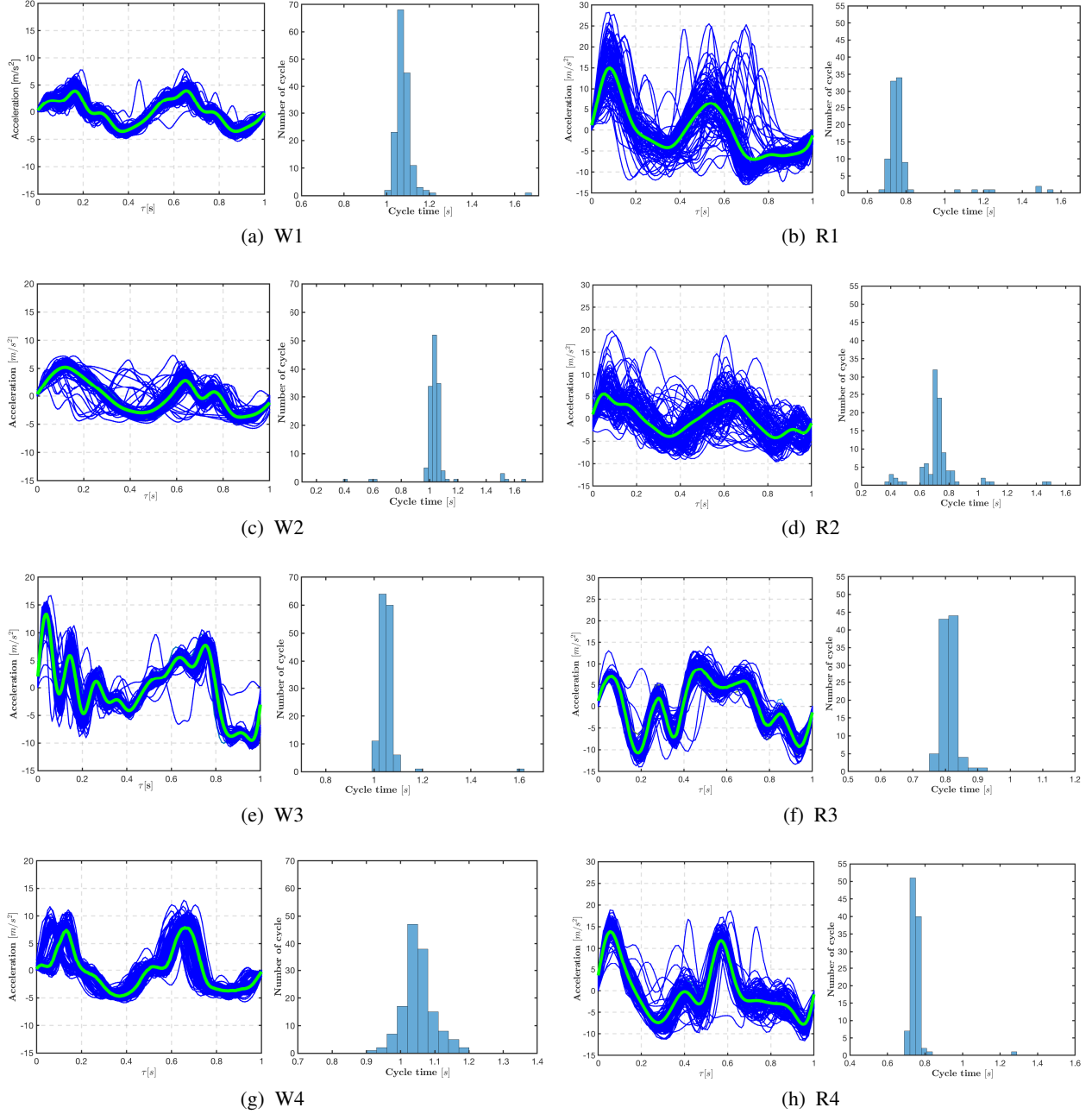


Figure 2: Results for all eight introduced scenarios in Table 2. In each sub-figure: On the right, detected gait cycles (blue lines) using Algorithm 2 are presented and estimated reference signal $\bar{\mathbf{g}}(\tau)$ is depicted on top of all detected gait cycles with a solid thick green line. On the left, the histogram for the gait cycle duration time is presented.

where θ is a vector containing all unknown coefficients, $\theta_K^{2K \times 1} = [a_0, a_1, \dots, a_{K-1}, b_0, b_1, \dots, b_{K-1}]^\top$, and $\bar{\mathbf{g}}^{L \times 1} = [\bar{\mathbf{g}}(\tau_0), \bar{\mathbf{g}}(\tau_1), \dots, \bar{\mathbf{g}}(\tau_{L-1})]^\top$. $\mathbf{H}_K^\top \in \mathbb{R}^{2K \times L}$ can then be given by

$$\mathbf{H}_K^\top = \begin{bmatrix} 1 & \cos(2\pi\tau_1) & \dots & \cos(2\pi\tau_{L-1}) \\ \vdots & \vdots & \dots & \vdots \\ 1 & \cos(2\pi\tau_1(K-1)) & \dots & \cos(2\pi\tau_{L-1}(K-1)) \\ 0 & \sin(2\pi\tau_1) & \dots & \sin(2\pi\tau_{L-1}) \\ \vdots & \vdots & \dots & \vdots \\ 0 & \sin(2\pi\tau_1(K-1)) & \dots & \sin(2\pi\tau_{L-1}(K-1)) \end{bmatrix}.$$

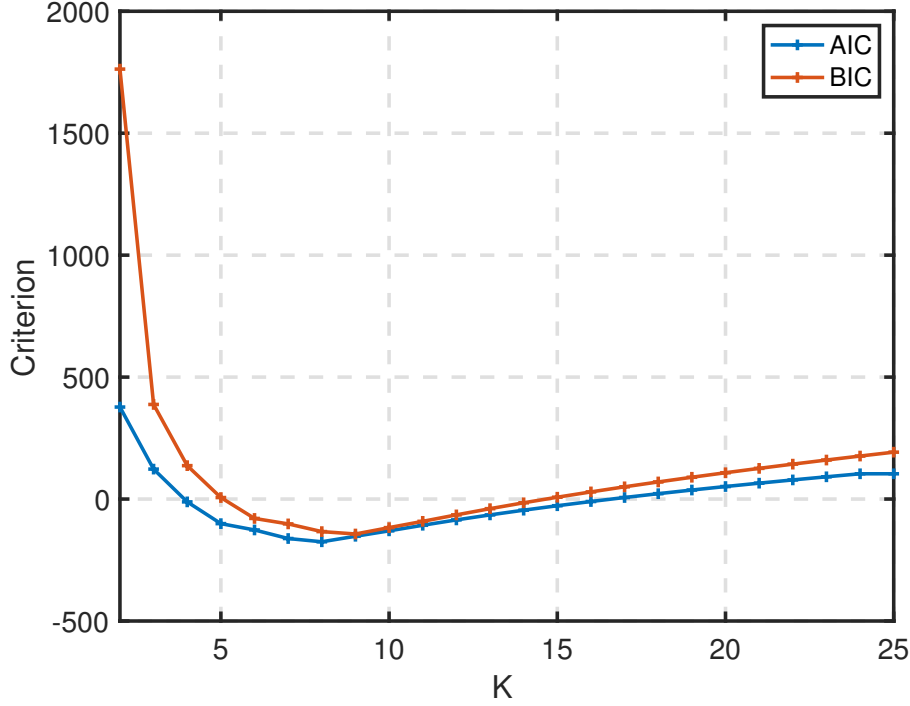


Figure 3: Model order selection.

The solution to the problem is obtained by finding the following optimization problem

$$\hat{\boldsymbol{\theta}} = \underset{\boldsymbol{\theta}}{\text{minimize}} \quad V^{LS}(\boldsymbol{\theta}), \quad (13)$$

where

$$V^{LS}(\boldsymbol{\theta}_K) = (\bar{\mathbf{g}} - \mathbf{H}_K \boldsymbol{\theta}_K)^\top (\bar{\mathbf{g}} - \mathbf{H}_K \boldsymbol{\theta}_K). \quad (14)$$

Finally, the closed form solution $\hat{\boldsymbol{\theta}}$ is given by

$$\hat{\boldsymbol{\theta}}_K = (\mathbf{H}_K^\top \mathbf{H}_K)^{-1} \mathbf{H}_K^\top \bar{\mathbf{g}}. \quad (15)$$

To find the best order model in FS expansion the gait cycle is modeled for $K \in [1, \dots, 25]$. Then, the FS coefficients, for each K are estimated and further evaluated by two well-known model selection criteria: Akaike information criterion (AIC) and Bayesian information criterion (BIC). Both AIC and BIC add a penalty term to their objective function. The difference between the two criteria is that BIC imposes a greater penalty for the number of parameters compared to AIC Fabozzi et al. [2014]. For a sample of size L , for each model order K , AIC and BIC are defined as

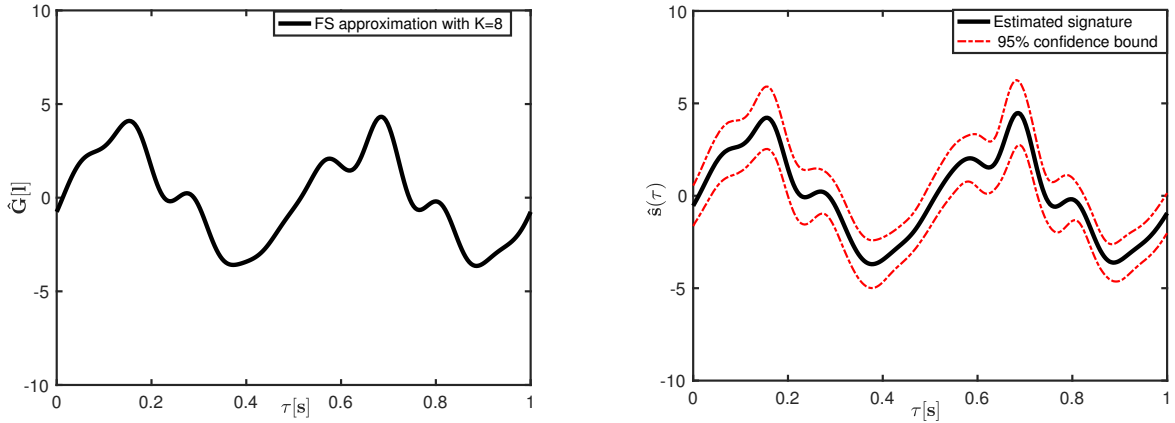
$$AIC = -2 \log p(\bar{\mathbf{g}} | \hat{\boldsymbol{\theta}}_K) + 2K, \quad (16a)$$

$$BIC = -2 \log p(\bar{\mathbf{g}} | \hat{\boldsymbol{\theta}}_K) + K \log L, \quad (16b)$$

where $p(\bar{\mathbf{g}} | \hat{\boldsymbol{\theta}}_K) = \mathcal{N}(\mathbf{H}_K \hat{\boldsymbol{\theta}}_K, \mathbf{H}_K (\mathbf{H}_K^\top \mathbf{H}_K)^{-1} \mathbf{H}_K^\top)$.

As Fig. 3 suggests, $K = 8$ and $K = 9$ are the suitable model orders for the gait segments presented in Fig. 1 according to AIC and BIC, respectively. While either of the two orders could be selected as the suitable model order for this scenario, we select the lower order, $K = 8$. Hence, the corresponding signatures can be generated by only incorporating $2K = 16$ estimated coefficients of the FS, $\hat{\boldsymbol{\theta}}$, into (11), as shown in Fig. 4a. Fig. 4b presents the gait signature $\bar{\mathbf{g}}(\tau)$, and its 95% confidence bound. As this figure shows, the averaging error has quite wide variance.

To evaluate the encoded signal by the estimated FS coefficients with 16 components, the approximate error between $\hat{\mathbf{G}}[l]$ and $\bar{\mathbf{g}}(\tau)$ are computed and illustrated in Fig. 5. As the result indicates, the approximation error is quite small with



(a) FS approximate of the signature generated by (11) for $K=8$.

(b) Estimated signature using (4).

Figure 4: Comparison between the estimated signature and its FS expansion.

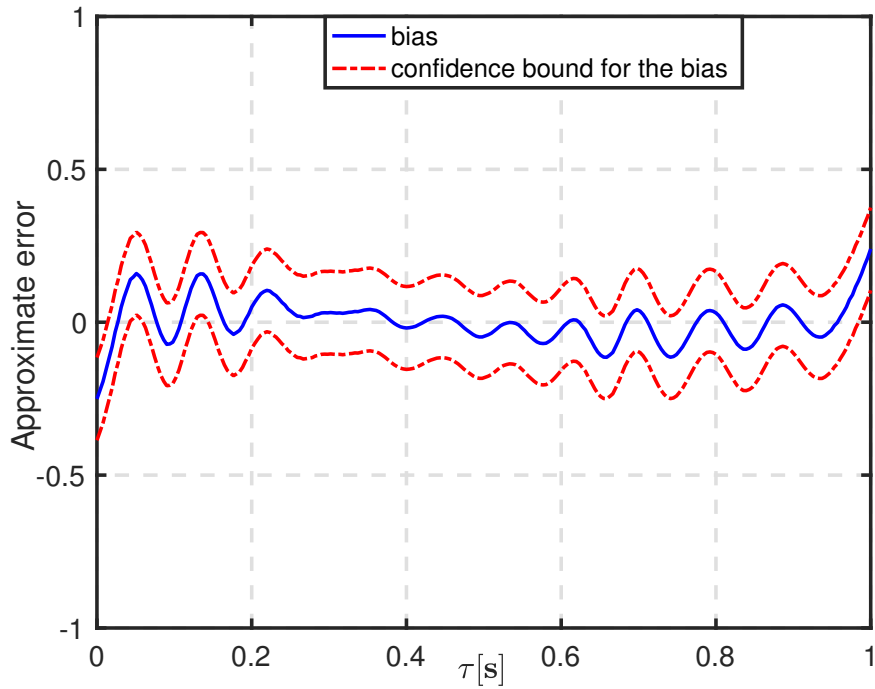


Figure 5: The approximation error and the 95% confidence bound.

narrow confidence bounds. That is, the approximation error introduced by the low order FS expansion is negligible compared to the averaging error. Subsequently, this low-dimensional feature vector together with the final least square cost value and the step time variations could provide a useful set of features for future classification purposes.

5 Experimental Results

In this section, the proposed method introduced in Sec. 3 is evaluated on several experimental data. Additionally, the data collection setup, together with devices and all considered scenarios, is described in detail.

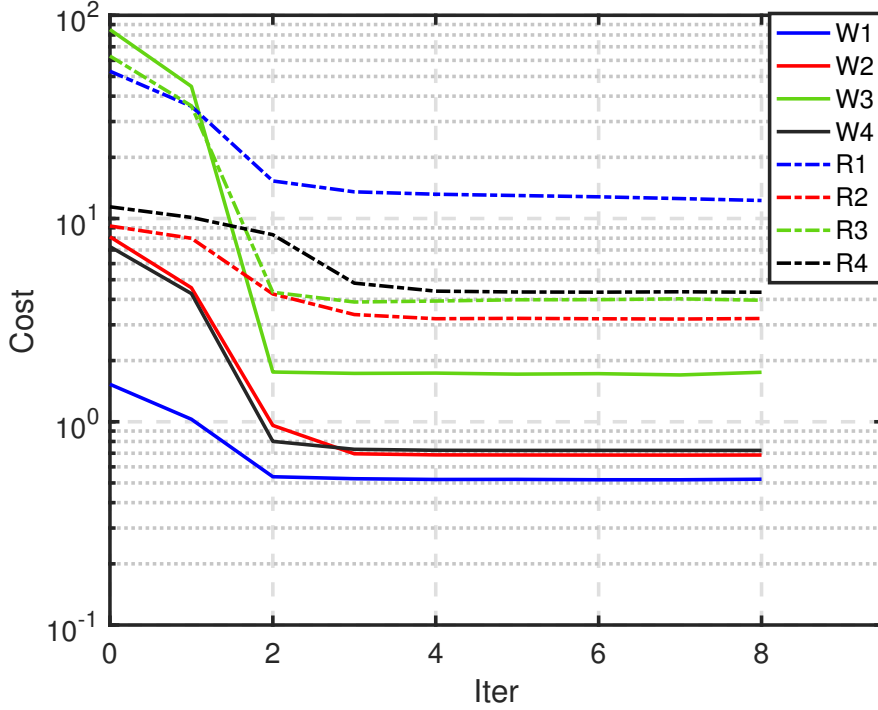


Figure 6: Evaluation $V(t_0:t_M)$ in (6) for eight iterations considering all scenarios in Table 2.

5.1 Data Description

In order to evaluate the performance of the proposed method, an extensive measurement campaign with different human motion modes and device poses has been designed. The sensor fusion Android app Linköping University, Sweden [2014], Hendeby et al. [2014] installed on a Nexus 5 was used to log accelerometer and gyroscope measurements with a sampling rate of 100 Hz. All the measurements were collected over the same trajectory, which was 249 m in length with four sharp corners in a parking lot at Linköping University. Several subjects with different attributes (gender, height and weight) participated in the experiment. The data was collected for multiple human activities and device modes. Table 2 summarizes all the experimental scenarios. To simplify referring to each of these scenarios, Table 2 also assigns a specific symbol to each of them Kasebzadeh et al. [2017].

5.2 Performance Evaluation

As the first step, the gait cycles for all the scenarios are detected using Algorithm 2 and illustrated in Fig. 2 together with estimated signatures which are computed based on (4).

Then, in order to fine-tune the gait segments extracted using the classical threshold-based algorithm, the proposed Algorithm 1 introduced in Sec. 3.1 is employed. The minimum and maximum of the most probable gait cycle times for each scenario, based on the histograms in Fig. 2, are used as a reference to define the upper and lower bounds in the optimization problem. The bounds are set to $\epsilon_{lo} = 0.5$ s and $\epsilon_{up} = 1.4$ s.

Table 2: Experimental scenarios.

Device mode	Motion mode	Walking (W)	Running (R)
	Fixed hand (1)		W1
Swinging hand (2)		W2	R2
Pocket (3)		W3	R3
Backpack (4)		W4	R4

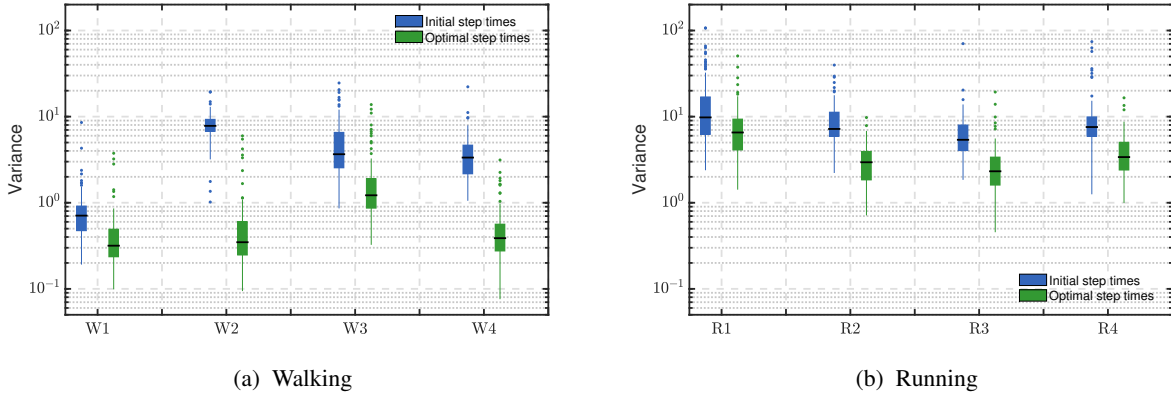


Figure 7: Variance of initial (blue) and tuned (green) gait cycles for all scenarios in Table 2.

Initial gait cycle times, obtained from Algorithm 2, are used to initialize the gait segmentation algorithm. Moreover, the initial signatures $\bar{g}(\tau)$ to be used in Algorithm 1 are estimated by (4) using the initial gait cycle times. It is worth noting that after each iteration, the signature $\bar{g}(\tau)$ will be updated by the tuned gait cycles. Fig. 6 presents the evaluated cost function for eight iterations of the optimization progress considering all scenarios introduced in Table 2. As the results indicate, in all scenarios after four iterations the cost function converges to the optimal values.

In order to evaluate how much the gait cycles are improved, the variance of all initial gait cycles with initial signature are compared with all optimal gait cycles with updated signatures. The distribution of the obtained variances is shown in Fig. 7. The box levels are 5%, 25%, 50%, 75%, and 95% quantiles and the asterisks show outlier values. As the figure suggests, for all scenarios the optimal variances are improved significantly and the mean of the variance of the optimal gait cycles is decreased notably. By comparing the walking mode in Fig. 7a the running mode one in Fig. 7b, it can be verified that running involves more unexpected movement for the device, hence there are more disturbances and it has a higher variance in total.

In order to give a better illustration of the performance of the proposed algorithm, we further examine “W2” and “R2” scenarios. The tuned gait cycles for these two scenarios are presented in Fig. 8. Comparing the results with initial gait cycles, see Fig. 2c and 2d, we realize that all the misdected gait cycles are properly detected, as indicated in the histograms Fig. 8b and 8d, and all the gait cycles are perfectly tuned.

The updated gait signatures for all eight scenarios in Table 2, obtained from the tuned gait cycles, together with their corresponding 95% confidence bounds, are presented in Fig. 9. As the figures suggest, the estimated gait signatures for all considered scenarios have a unique pattern. For walking modes, all signatures have a very narrow confidence bound which is a verification that the tuned gait cycles resemble the final gait signatures. The bound for running mode, however, is wider especially for the fixed hand device modes. This can also be verified by Fig. 7b, in which the variance of all optimal gait cycles for “R1” is higher than the other scenarios. This uncertainty can be explained by noting that users might have various unpredictable hand movements (especially while running) compared to the backpack and pocket scenarios in which the phone is more or less in a fixed position.

The updated signatures could be used for further investigation such as extracting low-dimensional feature vectors for the gait cycles. Twenty different model orders are applied to all introduced scenarios to find the best model order for each of them. The Bayesian information criterion for all 20 model orders are presented in Fig. 10. As shown in the figures, considering $K = 8$ for walking and $K = 10$ for running case would be suitable model orders to extract the feature vectors for the gait cycle in most cases, hence the signatures can be encoded efficiently. However, pocket mode in walking motion is the worst case from an FS perspective and requires $K = 10$.

Finally, the uniqueness of the signatures can be verified by investigating the scalar product of a pair of signatures. By doing so, it can be seen that the most unique signature corresponds to “W3” and that “R3” has the least similarity to the others. However, this is not always the case and there are cases that are not well separable from each other. For example, the signatures obtained for “W1”, “W4” and “R2” have higher correlation to each other.

In order to make the algorithm more automated, classification of the scenarios introduced in Table 2 would be an interesting topic for further investigation. For example, it is possible to consider the correlation of the gait signatures, given in Table 3, as inputs to the classifier. As a low hanging fruit, consider a classifier based on the highest correlation

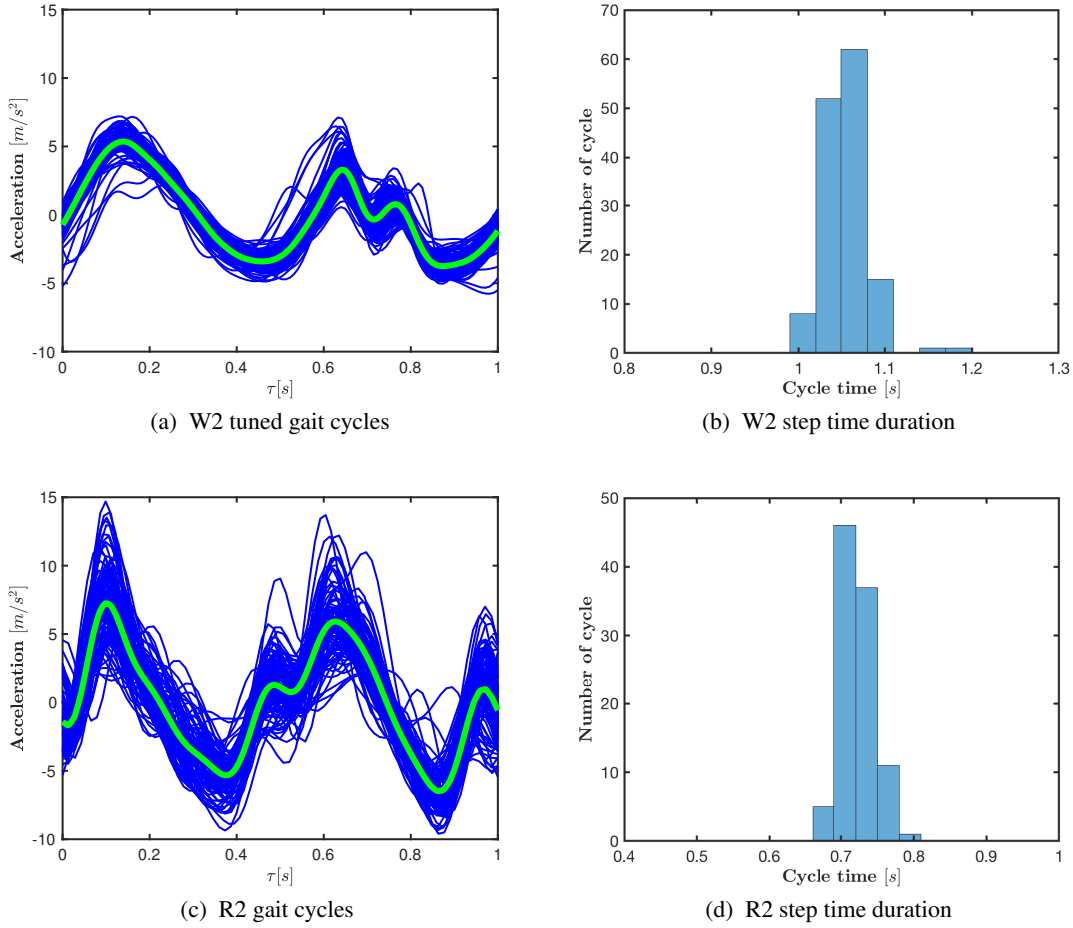


Figure 8: Optimized gait cycles with updated signatures for “W2” and “R2” introduced scenarios in Table 2.

score for which we achieved 70% classification accuracy. However, more sophisticated classifiers, *e.g.* those that consider temporal correlations in a filtering framework, would achieve much higher classification accuracies of 90-98%, see Kasebzadeh et al. [2019] for more detail.

6 Conclusion

Reliable pedestrian navigation systems require accurate step length estimation which in turn requires accurate gait cycle detection. In this work, an algorithm has been proposed for accurate gait cycle segmentation using IMU signals in multiple device and motion mode scenarios. For this purpose, we first used a classical thresholding algorithm to detect the gait cycles. Then, based on the asynchronous averaging of the gait cycles, a unique signature for each scenario was estimated. Furthermore, as a post-processing step, an optimization-based solution was proposed to tune the segmentation of the IMU signals in a way that minimized the variance of signature for each gait cycle. We showed that a Fourier series expansion of gait signatures provides a low-dimensional feature vector which could possibly be highly beneficial together with the final least square cost value and the step time variations for classification purposes. The performance of the proposed method has been evaluated using measurements collected from IMUs embedded in smartphones for different motion modes while being carried in different device modes. The results indicate good performance for the gait cycle segmentation problem for all of the considered scenarios.

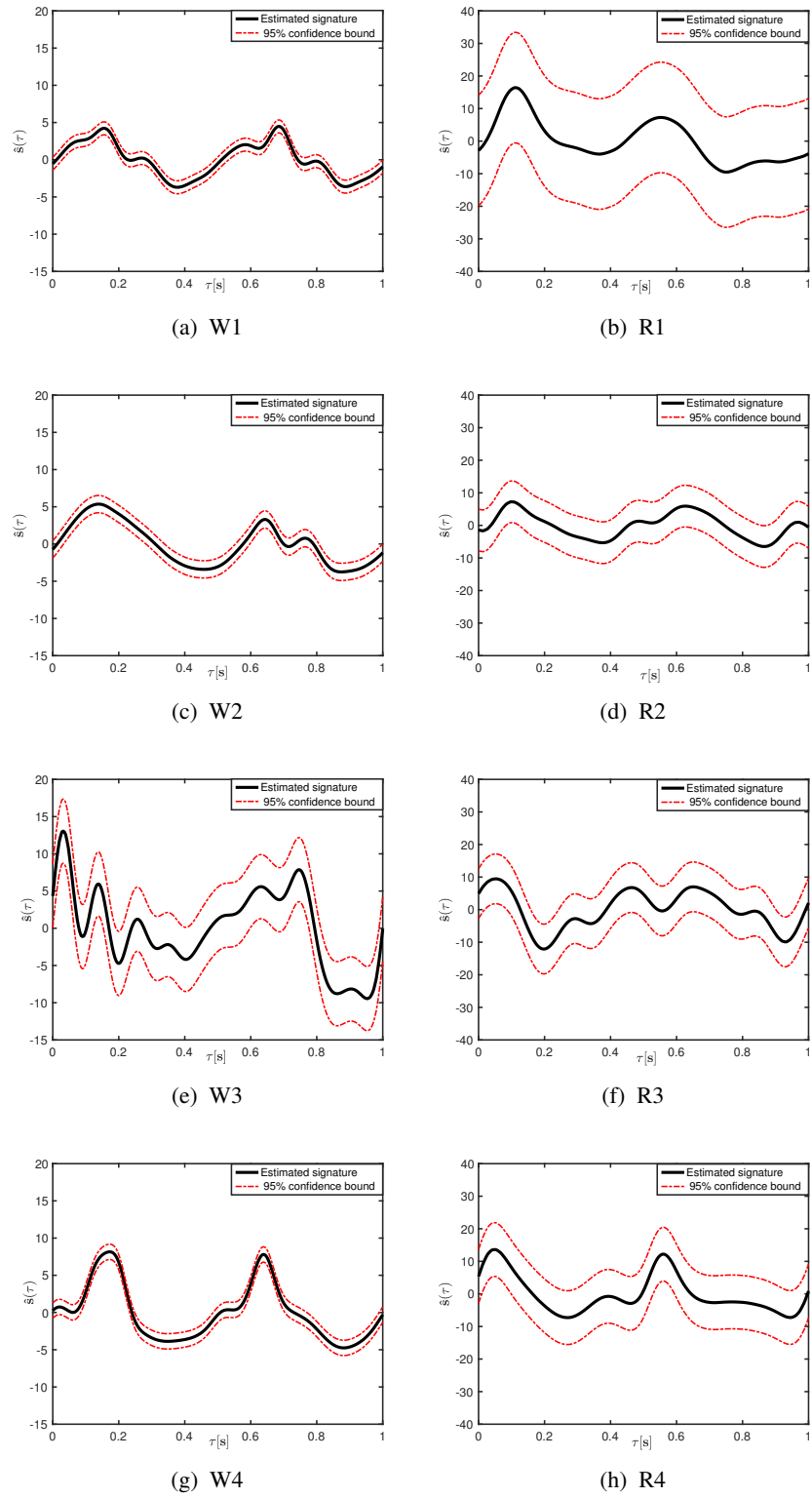


Figure 9: Gait signatures for all eight scenarios introduced in Table 2 [top] walking, [bottom] running.

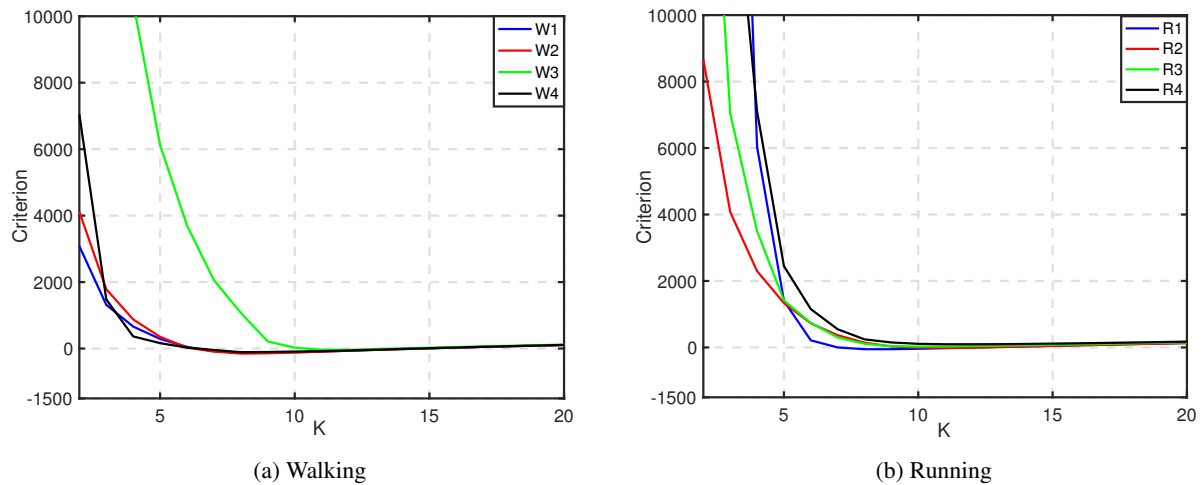


Figure 10: Model order selection using BIC.

Table 3: Correlation matrix for different signatures.

		Classes							
		W1	W2	W3	W4	R1	R2	R3	R4
Classes	W1	1	0.81	0.46	0.84	0.58	0.82	0.26	0.47
	W2	0.81	1	0.32	0.82	0.59	0.66	0.01	0.29
	W3	0.46	0.32	1	0.43	0.32	0.44	0.39	0.39
	W4	0.84	0.82	0.43	1	0.60	0.80	0.09	0.35
	R1	0.5	0.59	0.32	0.60	1	0.68	0.19	0.66
	R2	0.82	0.66	0.44	0.80	0.68	1	0.37	0.50
	R3	0.26	0.01	0.39	0.09	0.19	0.37	1	0.57
	R4	0.47	0.29	0.39	0.35	0.66	0.50	0.57	1

7 Acknowledgments

The author would like to thank PhD students from Linköping University who voluntarily participated in the data collection experiment.

This work is funded by the European Union FP7, the Marie Curie training program on *Tracking in Complex Sensor Systems* (TRAX) with grant number 607400, and the Swedish Research Council project *Scalable Kalman Filter*.

References

- A.K. Chowdhury, D. Tjondronegoro, V. Chandran, and S.G. Trost. Physical activity recognition using posterior-adapted class-based fusion of multiaccelerometer data. *IEEE J Biomed Health Inf*, 22(3):678–685, May 2018.
- C. Caramia, D. Torricelli, M. Schmid, A. M. Gonzalez, G. J. Vargas, F. Grandas, and J. L. Pons. IMU-based classification of Parkinson’s disease from gait: A sensitivity analysis on sensor location and feature selection. *IEEE J. Biomed. Health. Inf.*, 22(6):1765 – 1774, August 2018.
- A. R. J. Ruiz, F. S. Granja, J. C. P. Honorato, and J. I. G. Rosas. Accurate pedestrian indoor navigation by tightly coupling foot-mounted IMU and RFID measurements. *IEEE Trans. Instrum. Meas.*, 61(1):178–189, January 2012.
- Z. Tian, Y. Zhang, M. Zhou, and Y. Liu. Pedestrian dead reckoning for MARG navigation using a smartphone. *EURASIP Journal on Advances in Signal Processing*, 16(1):2–11, 2014.

- P Davidson and R. Piche. A survey of selected indoor positioning methods for smartphones. *IEEE Communications Surveys & Tutorials*, 19(2):1347–1370, May 2017.
- A. Jiménez, F. Zampella, and F. Seco. Improving inertial pedestrian dead-reckoning by detecting unmodified switched-on lamps in buildings. *Sensors*, 14(1):731–769, January 2014.
- J.-O. Nilsson, J. Rantakokko, P. Händel, I. Skog, M. Ohlsson, and K.V.S. Hari. Accurate indoor positioning of firefighters using dual foot-mounted inertial sensors and inter-agent ranging. In *IEEE/ION Position, Location and Navigation Symposium - PLANS 2014*, Monterey, CA, USA, May 2014.
- J. C. Alvarez, D. Alvarez, A. López, and R. C. González. Pedestrian navigation based on a waist-worn inertial sensor. *Sensors*, 12(8):10536–10549, 2012.
- I. Skog, P. Handel, J.O. Nilsson, and J. Rantakokko. Zero-velocity detection—an algorithm evaluation. *IEEE Trans Biomed Eng*, 57(11):2657–2666, November 2010.
- Q. Zeng, S. Zeng, J. Liu, Q. Meng, R. Chen, and H. Huang. Smartphone heading correction based on gravity assisted and middle time simulated-zero velocity update method. *Sensors*, 18(10), October 2018.
- G. Panahandeh, N. Mohammadiha, A. Leijon, and P. Händel. Continuous hidden Markov model for pedestrian activity classification and gait analysis. *IEEE Trans. Instrum. Meas.*, 62(5):1073–1083, May 2013.
- M. Basso, M. Galanti, G. Innocenti, and D. Miceli. Pedestrian dead reckoning based on frequency self-synchronization and body kinematics. *IEEE Sensors Journal*, 17(2):534–545, January 2017.
- R. Jirawimut, P. Ptasinski, V. Garaj, F. Cecelja, and W. Balachandran. A method for dead reckoning parameter correction in pedestrian navigation system. *IEEE Trans. Instrum. Meas.*, 52:209–215, 2003. ISSN 0018-9456.
- N. Ho, P. Truong, and G. Jeong. Step-detection and adaptive step-length estimation for pedestrian dead-reckoning at various walking speeds using a smartphone. *Sensors*, 16(9):1–13, September 2016.
- S. Zihajezadeh, T.J. Lee, J.K. Lee, R. Hoskinson, and E.J. Park. Integration of MEMS inertial and pressure sensors for vertical trajectory determination. *IEEE Trans. Instrum. Meas.*, 64(3):804–814, March 2015.
- L.E. Diez, A. Bahillo, J. Otegui, and T. Otim. Step length estimation methods based on inertial sensors: A review. *IEEE Sensors Journal*, 18(17):6908–6926, September 2018.
- K. Brzostowski. Toward the unaided estimation of human walking speed based on sparse modeling. *IEEE Trans. Instrum. Meas.*, 67(6):1389–1398, February 2018.
- A. Norrdine, Z. Kasmi, and J. Blankenbach. Step detection for ZUPT-aided inertial pedestrian navigation system using foot-mounted permanent magnet. *IEEE Sensors Journal*, 16(17):6766–6773, September 2016.
- P. Kasebzadeh, C. Fritsche, G. Hendeby, F. Gunnarsson, and F. Gustafsson. Improved pedestrian dead reckoning positioning with gait parameter learning. In *International Conference on Information Fusion*, Heidelberg, Germany, July 2016.
- V. Renaudin, M. Susi, and G. Lachapelle. Step length estimation using handheld inertial sensors. *Sensors*, 12(7):8507–8525, 2012.
- W. Kang and Y. Han. SmartPDR: Smartphone-based pedestrian dead reckoning for indoor localization. *IEEE Sensors Journal*, 15(6):2906–2916, May 2015.
- I. P. I. Pappas, M. R. Popovic, T. Keller, V. Dietz, and M. Morari. A reliable gait phase detection system. *IEEE Trans. Neural Syst. Rehabil*, 9(2):113–125, June 2001.
- H. Zhang, W. Yuan, Q. Shen, T. Li, and H. Chang. A handheld inertial pedestrian navigation system with accurate step modes and device poses recognition. *IEEE Sensors Journal*, 15(3):1421–1429, 2015.
- Z. Zhang, Y. Li, C. Peng, D. Mou, M. Li, and W. Wang. The height-adaptive parameterized step length measurement method and experiment based on motion parameters. *Journal Sensors*, 18(4):1039–1050, March 2018.
- A. Martinelli, H. Gao, P.D. Groves, and S. Morosi. Probabilistic context-aware step length estimation for pedestrian dead reckoning. *IEEE Sensors Journal*, 18(4):1600–1611, February 2018.

- Y. Li, Y. Zhuang, P. Lan, Hand Zhang, X Niu, and N. El-Sheimy. Self-contained indoor pedestrian navigation using smartphone sensors and magnetic features. *IEEE Sensors Journal*, 16(19):7173 – 7182, October 2016.
- J. Nocedal and S. J. Wright. *Numerical Optimization*. Springer, 2006.
- R.W. Levi and T. Judd. Dead reckoning navigational system using accelerometer to measure foot impacts, 1996.
- F. J. Fabozzi, S. M. Focardi, S. T. Rachev, and B. G. Arshanapalli. *The Basics of Financial Econometrics: Tools, Concepts, and Asset Management Applications*. John Wiley & Sons, 2014.
- Linköping University, Sweden. Sensor fusion app, December 2014. URL <https://goo.gl/0qNyU>.
- G. Hendeby, F. Gustafsson, and N. Wahlström. Teaching sensor fusion and Kalman filtering using a smartphone. In *Proceedings of the 19th IFAC World Congress*, Cape Town, South Africa, August 2014.
- P. Kasebzadeh, G. Hendeby, C. Fritsche, F. Gunnarsson, and F. Gustafsson. IMU dataset for motion and device mode classification. In *8th International Conference on Indoor Positioning and Indoor Navigation (IPIN2017)*, Sapporo, Japan, September 2017.
- P. Kasebzadeh, K. Radnosrati, G. Hendeby, and F. Gustafsson. Joint pedestrian motion state and device pose classification. *IEEE Trans Instrum Meas*, 2019.